I&EC research
Industrial & Engineering Chemistry Research

Article

pubs.acs.org/IECR

Chemistry and Kinetics of Heterogeneous Reaction Mechanism for Chemical Vapor Infiltration of Pyrolytic Carbon from Propane

Z. P. Tang,[†] A. J. Li,*[,†] Z. W. Zhang,[‡] X. Ma,[†] W. Wang,[†] J. M. Fang,[‡] and R. C. Bai[†]

[†]Research Center for Composite Materials, Shanghai University, 200072 Shanghai, China

[‡]National Key Laboratory of Advanced Functional Composite Materials, Aerospace Research Institute of Materials and Processing Technology, 100076 Beijing, China

Supporting Information

ABSTRACT: A heterogeneous reaction mechanism based on elementary reaction steps is proposed for the prediction of pyrolytic carbon deposition in chemical vapor infiltration, involving 72 surface species and 277 surface elementary reactions. A "prototype" gas-phase reaction is chosen to match with the corresponding surface reaction, and correction methods for kinetic data are also proposed for three kinds of surface reactions (i.e., surface/gas reactions, unimolecular surface reactions, surface/surface reactions) in the present work. Simulation results of deposition kinetics and gas-phase compositions of propane pyrolysis are validated by previously published experimental results of Marquaire's group, with a surface to volume ratio from 5 to 175 cm^{-1} and temperature from 1173 to 1323 K. The reaction pathways of the heterogeneous surface reactions and homogeneous gas-phase reactions are studied on the basis of the reaction flow rate analysis. An acceptable agreement indicates that the present heterogeneous reaction mechanism is reasonable, and acetylene, ethylene, and benzene are recognized as the main precursors of the pyrolytic carbon deposition at the present processing conditions.

1. INTRODUCTION

Carbon/carbon (C/C) composite synthesis involves the deposition of a matrix of pyrolytic carbon (pyrocarbon) produced by the pyrolysis of a gaseous hydrocarbon in a preform made of carbon fibers. This process is called chemical vapor infiltration (CVI).[1,2] The fundamentals of the process were first reviewed by Kotlenski 41 years ago.[3,4] Pyrolysis of propane is carried out at high temperature (i.e., 900−1500 K) and low pressure (i.e., 1−50 kPa). It produces, in addition to pyrocarbon, hydrogen and various hydrocarbons from light species, such as methane, to heavier species, such as polycyclic aromatic hydrocarbons (PAHs).[5,6]

Owing to the low deposition rates and mass transport limitations of precursors within the pores of the substrate when a gaseous hydrocarbon is fed to prepare C/C composites, the infiltration duration is long and consequently the costs are high.[7] As the residence time in the reactor is short, the gas-phase system can seldom realize thermodynamic equilibrium; thus the CVI process of hydrocarbon pyrolysis is dominated by rules of chemical kinetics. Researchers have made extensive achievements of the purely homogeneous reaction mechanism of hydrocarbon pyrolysis[8−10] in the past few decades, but what really happens on the surface of carbon fibers remains unknown. A sound knowledge of the homogeneous and heterogeneous reactions involved in pyrocarbon deposition might help decrease manufacturing costs of C/C composites by optimizing CVI processes.[11,12]

Li et al.[13,14] successfully simulated the CVI process by the lumped deposition model, considering ethylene, acetylene, and benzene as the main precursors of pyrocarbon. A similar approach was used by Ziegler et al.[15] to describe the deposition reactions of pyrocarbon, which avoided the description of the pyrocarbon surface in terms of surface species. The deposition reactions of the lumped mechanism are considered as direct dehydrogenation reactions from hydrocarbon species (e.g., C_nH_m), and these reactions are irreversible. Thus, the lumped reaction of deposition is written as

$$C_nH_m \rightarrow nC + \frac{m}{2}H_2$$

where C is the carbon atom constituting the graphene layers. Here the rate of the first-order deposition reaction is expressed as

$$r = nk[C_nH_m] \quad (1)$$

where k (s^{-1}) and r ($mol/cm^3 \cdot s$) are the rate constant and the rate of pyrocarbon deposition, respectively. The mass deposit rate r_{mass} (g/s) is known in the experimental results, V (cm^3) is the volume of the reactor, and M_c (12 g/mol) is the atomic molar mass of carbon; then

$$r = \frac{r_{mass}}{M_c V} \quad (2)$$

According to eqs 1 and 2, the rate constant is expressed as

$$k = \frac{r_{mass}}{n[C_nH_m]M_c V} \quad (3)$$

The rate constant k follows the Arrhenius equation, which is a function of temperature. By plotting the logarithm of experimental values of the rate constant according to the reciprocal of temperature, the pre-exponential factor and

Received: June 30, 2014
Revised: October 12, 2014
Accepted: October 20, 2014
Published: October 20, 2014

dx.doi.org/10.1021/ie5026024 | Ind. Eng. Chem. Res. 2014, 53, 17537−17546

activation energy of the deposition reaction were obtained. Adding the lumped deposition reactions to the homogeneous reaction mechanism, the gas-phase compositions including that of pyrocarbon were well reproduced by the simulation. The computing results of the molar fraction of pyrocarbon can then be converted into the mass of pyrocarbon deposited.

A model based on surface reactions on "active surface sites" was proposed by Becker and Hüttinger,[16−18] and the pyrocarbon deposition reactions were treated as lumped heterogeneous reactions including adsorptions, surface reactions, and desorptions. The gas-phase species in the lumped heterogeneous reactions of pyrocarbon deposition from C_2-hydrocarbon were summed up in three kinds of hydrocarbons (i.e., C_2-, C_4-, and C_6-hydrocarbons). The chemical-kinetic data were obtained by fitting simulated results with experimental results from the chemical vapor deposition (CVD) process. This model represents the first attempt to describe pyrocarbon deposition on the basis of the Langmuir−Hinshelwood mechanism with additional consideration of the complex gas-phase chemistry.

It is worth noting that these kinetic data of the lumped heterogeneous reactions are only usable in the given experimental conditions; therefore, a detailed mechanism consisting of surface elementary reactions attracts sufficient interest, which is applicable in comprehensive operational conditions without any modification. Previous work about detailed kinetic mechanisms to model diamond,[19] coke,[20] and pyrocarbon deposition[11] is a good benchmark for further research. Frenklach and Wang[19] introduced a model consisting of 158 irreversible gas-phase reactions and 52 irreversible surface elementary reactions to describe the diamond deposition from methane−hydrogen by a CVD process. They referred to the gaseous "prototype reaction", supposing the kinetic data of the surface elementary reactions were similar to the "prototype gas-phase reactions". The pre-exponential factor of the Arrhenius equation was modified by a correction factor derived from the collision theory. A similar approach was applied by Wauters and Marin[20] to model coke formation during steam cracking. According to the conclusion, abstraction of hydrogen atoms and the addition of radical surface species to alkenes have great effect on the coke formation rate. Marquaire et al.[11] further developed the method of gaseous "prototype reaction", and a heterogeneous reaction mechanism consisting of surface elementary reactions was presented to describe the pyrocarbon deposition for the first time. Good agreements were reached by confrontation of simulations and experiments for both deposition kinetics and gas-phase compositions, but there still existed some problems such as nonconservation of the surface sites in the heterogeneous reaction mechanism. A more flexible one will be proposed in the present work. The surface reaction pathways and related surface reactions are constructed and the correction methods for three kinds of surface reactions are introduced for the first time. The modeling methodology is discussed in section 3, and a detailed heterogeneous reaction mechanism is available in the Supporting Information.

The surface area of carbon fibers to the reactor volume ($[A_S/V_R]$) ratio and temperature are critical parameters in the CVI process of pyrocarbon. Changing these parameters causes variation of the deposition chemistry, the deposition kinetics, and the texture of deposited carbon.[21−23] In this study, the deposition kinetics of pyrocarbon from propane is simulated with different $[A_S/V_R]$ ratios and temperatures. According to the simulation, we can not only check the correctness of the heterogeneous reaction mechanism by comparing with the experimental results of Marquaire et al.,[11,24] but we also can narrow down the reaction pathways of the homogeneous gas-phase reactions and heterogeneous surface reactions during the propane pyrolysis in the CVI process by reaction flow rate analysis.

2. EXPERIMENTAL SECTION

The introduction of the jet stirred reactor is available in the experimental research of Marquaire et al.[11,24] The reactor consists of two parts, which are connected to each other. In the "low" part, there is a cylindrical support with a flat extremity on which carbon fibers can be laid. In the "high" part, the inlet gas is preheated and then injected into a cross composed of four nozzles, which produce a jet in four directions and ensure the gas is perfectly mixed. Therefore, the compositions of the gas phase close to the surface of carbon fibers during the pyrolysis are the same as the compositions in the space of the reactor.

The experimental setup is simplified to a *continuous stirred tank reactor* (CSTR), as shown in Figure 1, with a volume of

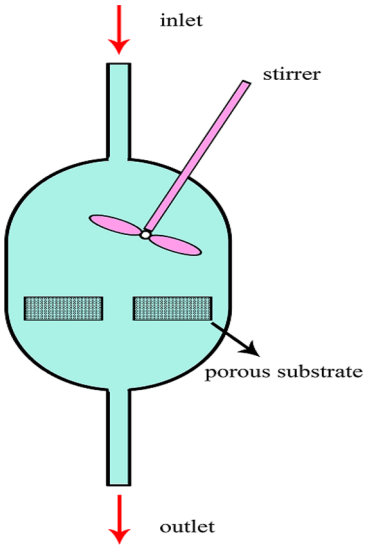

Figure 1. Schematic of the CSTR.

approximately 90 cm^3 and an internal area of 100 cm^2; thus its $[A_S/V_R]$ ratio is around 1.1 cm^{-1}. The deposition process is performed on a circular preform made of carbon fibers with a diameter of 7.5 μm. Processing parameters of the simulation are identical with the experimental ones.[11,24]

A mixed gas of propane and nitrogen with a mole ratio of 1/9 is pyrolyzed with a total pressure of 2.7 kPa. When the $[A_S/V_R]$ ratio is investigated, the temperature and residence time are set at 1273 K and 1 s, respectively. The $[A_S/V_R]$ ratio of the carbon preform varies from 25 to 175 cm^{-1}. A contrast experiment is performed when the reactor is empty and the $[A_S/V_R]$ ratio is 1.1 cm^{-1}. When the influence of temperature (1173−1323 K) is discussed, the residence time is fixed at 1 s. Two experiments are carried out: one is performed with a fibrous carbon preform (initial mass is around 1.3 g) and the $[A_S/V_R]$ ratio is 44 cm^{-1}; the other is performed without carbon preform in the reactor ($[A_S/V_R]$ ratio = 1.1 cm^{-1}) as a contrast experiment.

Marquaire et al. analyzed the compositions of light gas-phase species online by two gas chromatographs at the outlet of the reactor after the deposition process. The heavy species

dx.doi.org/10.1021/ie5026024 | Ind. Eng. Chem. Res. 2014, 53, 17537−17546

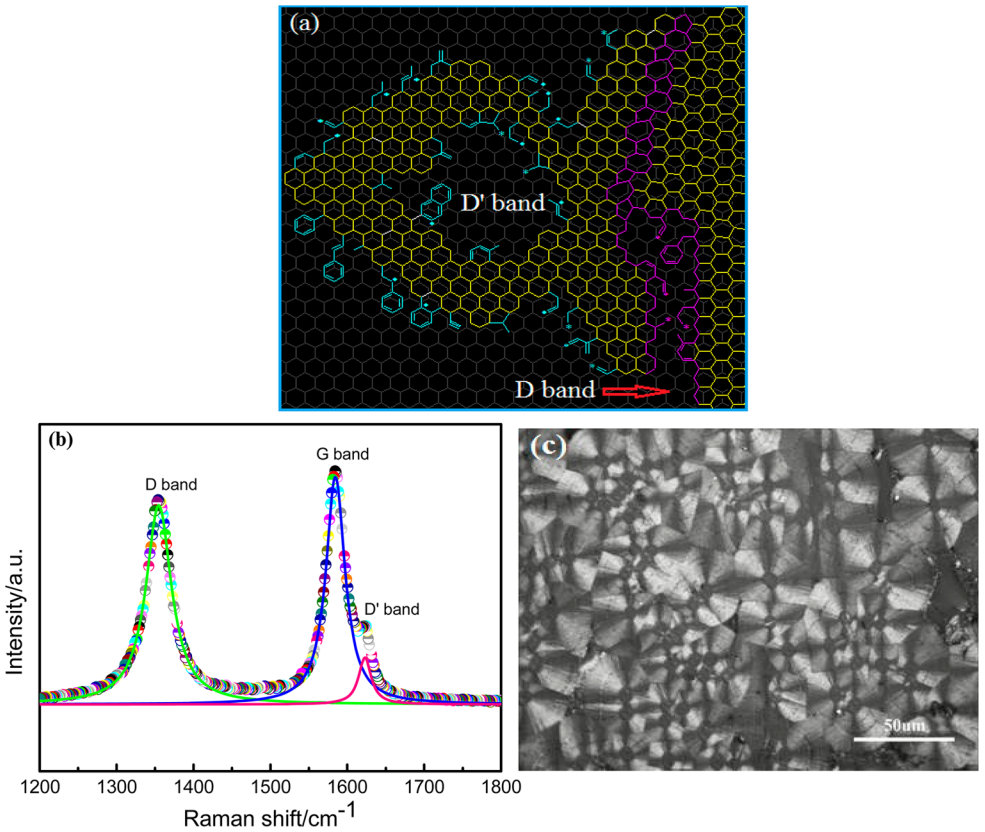

Figure 2. (a) Schematic drawing of lateral growth of BSUs on the pyrocarbon surface. (b) First-order Raman spectra of a medium-textured pyrocarbon. (c) Polarized light micrograph of the infiltrated sample corresponding to (b).

containing more than five carbon atoms are condensed in a cooled trap with liquid nitrogen, and the compositions of heavy gas-phase species are analyzed by a gas chromatograph after the deposition process. The mass of pyrocarbon deposited is measured by weighing the preform before and after the deposition. A detailed description of the experimental method is available in previous research.[24] The diffusion limitations in the gas-phase space and within the carbon fiber preform are estimated by calculating the external residence fraction and the Weisz modulus at the early stage of the CVI process. According to the results, the diffusion limitations are negligible in these conditions.[11]

3. MODELING METHODOLOGY

The homogeneous reaction mechanism containing 285 gas-phase species and 1074 gas-phase reactions of the propane pyrolysis in the CVD process is proposed on the basis of Norinaga's work[6] and Marquaire's work[15] by Xu et al.[12] Main reaction pathways and crucial reaction steps have been determined at 1248 K for a residence of 1 s by the flow rate analysis. The significant roles of radicals such as propargyl, cyclopentadienyl, and indenyl in the formation of PAHs are discussed.

3.1. Description of Pyrocarbon Surface. In order to establish a heterogeneous reaction mechanism based on surface elementary reactions, the pyrocarbon surface has to be defined first. The contact surface between fibers of the preform is omitted and the preform is assumed to be a single cylindrical fiber with a diameter d and mass m; then the length of the fiber is

$$L = \frac{4m}{\rho\pi d^2} \tag{4}$$

Consequently, the contact area between the fiber and gas phase is

$$S = \pi dL \tag{5}$$

As the duration of the CVI process is relatively short, the value of S is assumed to be constant in the modeling. The surface site density Γ (mol/cm^2) is required in the simulation,[25] and it is a constant value. In the light of the estimation method of Marquaire et al.,[11] we consider only the carbon atoms located at the edge of basic structural units (BSUs) as active sites. The value of 8×10^{14} sites/cm^2 is used in the work; i.e., the surface site density is approximately 1.45×10^{-9} mol/cm^2. All surface reactions occur simultaneously in the hypothetical flat surface, e.g., adsorptions, desorptions, and surface reactions. Figure 2a sketches the possible lateral growth of BSUs during the infiltration process. It is possible to form defects inside the ring or in the graphene grain boundaries (the purple-colored region). According to the first-order Raman spectra of a medium-textured pyrocarbon in Figure 2b, three Lorentzian peaks show good curve fittings of D (1355 cm^{-1}), G (1580 cm^{-1}), and D′ (1620 cm^{-1}) bands. A basic hypothesis is that the D and D′ bands are associated with the structural imperfection between the graphene grains and the defects inside the grains, respectively.[26−30] Figure 2c shows a polarized light micrograph of the infiltrated sample corresponding to Figure 2b.

3.2. Detailed Reaction Pathways. As surface elementary reactions occurring at the edge of BSUs are similar to the gas-phase reactions of aromatic species, we get inspiration from

elementary reactions involved in gas-phase pyrolysis: H-abstraction, addition of unsaturated species, β-scission, ipso addition, initiation, and termination reactions. Analogous reactions are assumed to occur at the edge of BSUs. According to the work of Marquaire et al.,[11] the surface sites are evenly split by armchair and zigzag sites (Figure 3). At least two

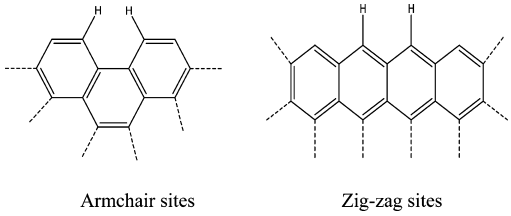

Figure 3. Armchair and zigzag surface sites.

carbon atoms are added on armchair sites to form a six-atom aromatic ring, while three carbon atoms are added on zigzag sites. There are 72 surface species specified in armchair and zigzag sites.

Two main reaction mechanisms have been proposed in heterogeneous catalysis, namely Langmuir−Hinshelwood[31] and Eley−Rideal.[32] In the Langmuir−Hinshelwood mechanism, the two surface species chemisorbed on the surface react with each other, whereas in the Eley−Rideal mechanism only one surface species is chemisorbed and the other one reacts with it directly from the gas phase, without adsorbing. Two reaction mechanisms are considered to describe pyrocarbon deposition in this work and three kinds of surface elementary reactions are proposed: surface/gas reactions, unimolecular surface reactions, and surface/surface reactions:

$$G + B(S) \rightarrow \text{products}$$

$$B(S) \rightarrow \text{products}$$

$$B(S) + C(S) \rightarrow \text{products}$$

where G, B(S), and C(S) represent gas-phase species and surface species, respectively. The detailed reaction pathways of the heterogeneous reaction mechanism refer to Marquaire et al.,[11] Bohm et al.,[33] Dong et al.,[34] and Norinaga et al.,[35] involving the main molecules and radicals in the gas phase during hydrocarbon pyrolysis. There are 277 surface elementary reactions with the conservation of surface sites in the heterogeneous reaction mechanism.[25] All these surface reactions are proposed in an irreversible format[25] and "dummy" values of thermodynamic data are employed during numerical calculations.[25] For more details, please refer to the Supporting Information.

3.3. Correction Methods. When detailed reaction pathways and related surface elementary reactions are proposed at first, no kinetic data of each surface reaction are available. A gas-phase elementary reaction chemically close to the surface reaction is chosen as the "prototype" reaction of a surface elementary reaction.[11] The prototype gas-phase reaction and its related kinetic data are obtained from the NIST Chemical Kinetics Database or related literature. The activation energies of surface elementary reactions are equal to those of prototype gas-phase reactions, while the pre-exponential factors may be modified, resulting from the steric hindrance of graphene stacks. The correction methods for kinetic data of surface elementary reactions are founded on the premise that chemical reactivity of solid carbonaceous materials localized on the carbon sites is similar, in a manner, to that of the corresponding gaseous species.[19]

3.3.1. Surface/Gas Reactions and Unimolecular Surface Reactions. Through ab initio method,[36] the influence of the size of an aromatic species on the pre-exponential factor of the Arrhenius equation is negligible in the formation of PAHs; consequently, gas-phase reactions containing a molecule of benzene or its derivatives are used as "prototype reactions" to estimate kinetic data of surface/gas reactions or unimolecular surface reactions. However, the high yields of PAHs and low yields of pyrocarbon in the CVD study[34,37,38] hint that the steric effects should be stronger in the case of surface reactions occurring at the edges of graphene layers. Therefore, if the prototype gas-phase reaction contains a molecule of benzene or its derivatives, the pre-exponential factor of the surface elementary reaction will be reduced to 0.1, as shown in Table 1. The correction factor proves to be reasonable by comparing the simulated results with the experimental results as shown in section 4.

Table 1. Surface Elementary Reaction and Its Prototype Reaction Involving Benzene

Surface Reaction: C_(S) + C_2H_2 → CHCH_(S)				
	prototype reaction rate const k_g			
prototype gas-phase reaction	A (cm, mol, s)	n	E_a (kJ/mol)	ref for k_g and comments
$C_6H_5 + C_2H_2 \rightarrow C_6H_5 + C_2H_2$	2.69×10^6	2.05	15.55	$k_s = 0.1k_g$[39]

However, some prototype gas-phase reactions involving a molecule of benzene or its derivatives are not available in the literature. In analogy with some gas-phase reactions in the chemistry of PAHs, the kinetic data are not obtained experimentally and theoretically but rather are estimated by their prototype reactions of small unsaturated molecules (e.g., acetylene or ethylene).[5,40] By applying a correction factor derived from collision theory, Frenklach and Wang[19] calculated the kinetic data of surface elementary reactions based on prototype gas-phase reactions of small molecules. Theoretically, the chemical reactivity of active sites at the graphene layers is similar to that of the reactive moiety in corresponding prototype gaseous species. The rate constant of the gas/surface reactions (the most common reactions in the pyrocarbon formation network) is modified by a correction factor λ:

$$k_s = \lambda k_g \tag{6}$$

where k_s and k_g are the rate constants of the surface elementary reaction and the prototype gas-phase reaction, respectively.

$$\lambda = \frac{\Omega_s}{4\Omega_g\left[1 + \frac{m_p}{m_g}\right]^{1/2}} \tag{7}$$

$$\Omega_g = \frac{\pi(d_g + d_p)^2}{4} \tag{8}$$

Equation 8 is valid for a bimolecular surface reaction between a gaseous species "g" and a surface species represented by a prototype gas-phase species "p". Ω_g is the collision cross section of the prototype gas-phase reaction; d_g and d_p are the diameters of the gaseous reactant and prototype gaseous species. The

dx.doi.org/10.1021/ie5026024 | Ind. Eng. Chem. Res. 2014, 53, 17537−17546

collision cross section of the surface species Ω_s in the present study is 2.6 Å^2/site for pyrocarbon surface.[20] The correction factors of the surface/gas reactions are in the range 10^{-3}–10^{-2}, and an example is shown in Table 2.

Table 2. Surface/Gas Reaction and Its Prototype Reaction with a Correction Factor

Surface Reaction: $C_2H_4(S) + CH_3 \rightarrow C_2H_3\_(S) + CH_4$				
	prototype reaction rate const k_g			
prototype gas-phase reaction	A (cm, mol, s)	n	E_a (kJ/mol)	ref for k_g and comments
$C_2H_4 + CH_3 \rightarrow C_2H_3 + CH_4$	4.16×10^{12}	0	46.40	$k_s = 0.008k_g$[41]

The determination of the rate constant of unimolecular surface reactions is based on the assumption that equilibrium constants of surface reactions are equal to those of the corresponding prototype gas-phase reactions. The correction factor for the unimolecular surface reaction is, therefore, equal to that of its reverse reaction. Because a reverse bimolecular reaction can be written down for any unimolecular surface reaction in the pyrocarbon deposition network, the correction factor for this reverse reaction and thus for the unimolecular surface reaction can then be calculated via eq 7. An example is shown in Table 3.

Table 3. Unimolecular Surface Reactions and Prototype Reactions with Correction Factors

Surface Reactions: (1) $C_2H_4(S) \rightarrow C_2H_3\_(S) + H$; (2) $C_2H_3\_(S) + H \rightarrow C_2H_4(S)$				
	prototype reaction rate const k_g			
prototype gas-phase reaction	A (cm, mol, s)	n	E_a (kJ/mol)	ref for k_g and comments
(1) $C_2H_4 \rightarrow C_2H_3 + H$	4.16×10^{12}	0	46.4	$k_s = 0.0041k_g$[42]
(2) $C_2H_3 + H \rightarrow C_2H_4$	3.88×10^{13}	0.2	0	$k_s = 0.0041k_g$[43]

3.3.2. Surface/Surface Reactions. A prototype gas-phase reaction cannot be found for a bimolecular reaction of two neighboring surface species A(S) and B(S), as shown in Figure 4. In this case, a cyclization reaction between two neighboring surface species, such as $C_2H_2\_(S)$ and H(S), is proposed:

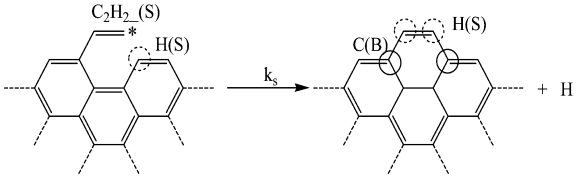

Figure 4. Surface/surface reaction.

$$C_2H_2\_(S) + H(S) \xrightarrow{k_s} 2C(B) + 2H(S) + H$$

$$r = k_s[C_2H_2\_(S)][H(S)]S \quad (9)$$

$$r_1 = k_c[C_2H_2\_(S)]z\_H(S)S = k_g[C_2H_2\_(S)]z\_H(S)S \quad (10)$$

$$z\_H(S) = [H(S)]\delta_{H(S)}/\Gamma \quad (11)$$

The rate constant of the surface reaction is k_s (cm^2/mol·s), and the rate constant of the cyclization reaction k_c (s^{-1}) equals the rate constant of the prototype gas-phase reaction k_g (cm^3/mol·s). [H(S)] (mol/cm^2) and z_H(S) are the concentration and the mole fraction of surface species H(S), respectively. S (cm^2) represents the preform area, Γ is the surface site density (1.45×10^{-9} mol/cm^2), and $\delta_{H(S)}$ is the number of sites the surface species H(S) occupies. Here $\delta_{H(S)} = 1$, for each surface species occupies only one site before the cyclization reaction. Considering the above equations and $r = r_1$, we have

$$k_s = k_g/\Gamma \quad (12)$$

Here we assume the formation of benzene and hydrogen atom from linear C_6H_7 as the prototype gas-phase reaction, as shown in Figure 5. The kinetic data of the prototype gas-phase reaction and the correction factor are listed in Table 4.

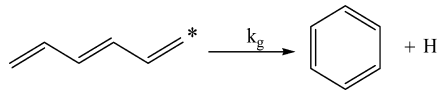

Figure 5. Prototype gas-phase reaction.

Table 4. Surface/Surface Reaction and Its Prototype Reaction with a Correction Factor

Surface Reaction: $C_2H_2\_(S) + H(S) \rightarrow 2C(B) + 2H(S) + H$				
	prototype reaction rate const k_g			
prototype gas-phase reaction	A (cm, mol, s)	n	E_a (kJ/mol)	ref for k_g and comments
$C_6H_7 \rightarrow C_6H_6 + H$	8.4×10^{21}	−4.2	47.5	$k_s = k_g/\Gamma$[44]

The nomenclature of 72 surface species, the heterogeneous reaction mechanism of 277 reactions, and the prototype gas-phase reactions are all presented in the Supporting Information.

4. RESULTS AND DISCUSSION

4.1. Pyrocarbon Deposition. The influence of the $[A_S/V_R]$ ratio is discussed, according to the experimental results from Marquaire et al.[24] The deposition rate of pyrocarbon in the 120 min deposition duration equals the deposition rate of pyrocarbon in the 240 min deposition duration; i.e., the duration of infiltration does not influence the kinetics of deposition at the initial stage of pyrocarbon deposition. The deposition process of 120 min is simulated here, and the simulated results of the mass of pyrocarbon deposited are compared with the experimental results, as shown in Figure 6a. When the $[A_S/V_R]$ ratio is lower than 60 cm^{-1}, the mass of pyrocarbon deposited is well reproduced by the model. The deviation increases as the $[A_S/V_R]$ ratio increases, and a maximum error of 18.89% appears when the $[A_S/V_R]$ ratio reaches approximately 130 cm^{-1}. Although there are some numerical disparities compared to the experimental results, the variation tendency of the mass of pyrocarbon deposited as a function of the $[A_S/V_R]$ ratio can be well revealed by the present simulated results. Especially when the $[A_S/V_R]$ ratio is below 20 cm^{-1}, the mass of pyrocarbon drastically increases

dx.doi.org/10.1021/ie5026024 | Ind. Eng. Chem. Res. 2014, 53, 17537−17546

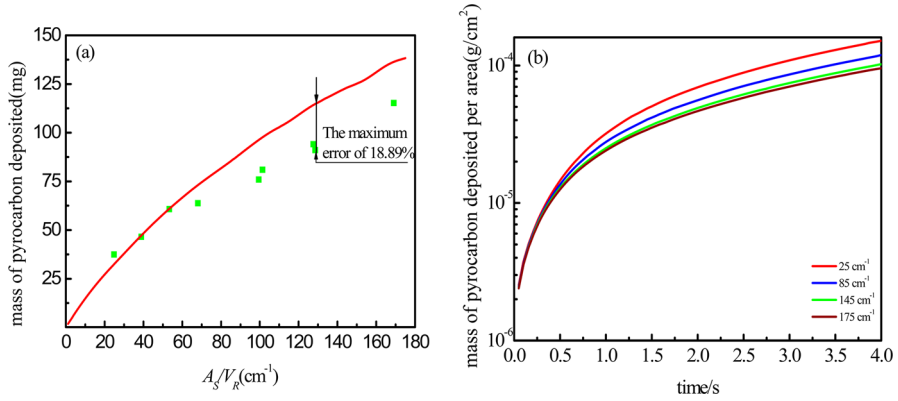

Figure 6. Influence of $[A_S/V_R]$ ratio on mass of pyrocarbon deposited (symbols, experimental results; lines, simulated results).

with the $[A_S/V_R]$ ratio. Figure 6b predicts the variation tendency of the mass of pyrocarbon deposited per area as a function of deposition time in different $[A_S/V_R]$ ratios: the mass of pyrocarbon deposited per area decreases with increasing $[A_S/V_R]$ ratio.[45]

The influence of temperature is studied using previously published experimental results from Marquaire et al.[11] The computational results of the pyrocarbon deposition rate are compared to the experimental data in Figure 7. When the temperature is lower than 1300 K, the mass of pyrocarbon deposited is well reproduced by the model. The deviation increases as temperature increases, and a maximum error of 25.01% appears when the temperature is approximately 1320 K. This implies that the activation energies of some deposition reactions are a little high. The higher the activation energy is, the faster the reaction rate increases when the temperature rises.

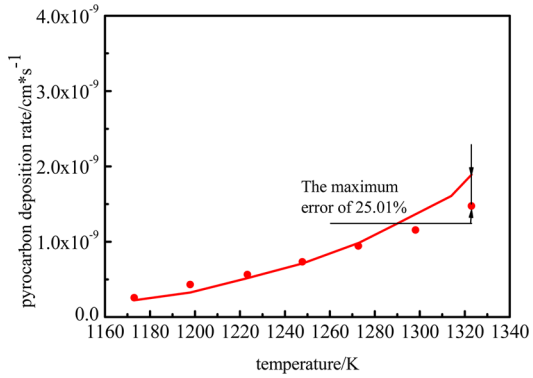

Figure 7. Comparison between (symbols) experimental and (line) computed pyrocarbon deposition rates as a function of temperature.

4.2. Compositions of Light Gas-Phase Species. According to the experimental results of light species after 2 h of deposition from Marquaire et al.,[24] the molar fractions of light species at the outlet of the reactor are well estimated using the kinetic mechanism we put forward, as shown in Figure 8. The formation of hydrogen is overpredicted for $[A_S/V_R]$ ratios above 100 cm^{-1}, and methane is slightly overpredicted for the entire range of $[A_S/V_R]$ ratios. Acetylene is underpredicted. This underestimation is explained by the high reaction rates for the acetylene consumption in the surface reactions. The prediction of ethylene is not satisfactory at both ends of the simulated curve, which may be from the experimental errors. Butadiene is well predicted, while but-1-ene-3-yne is underpredicted for the entire range of $[A_S/V_R]$ ratios. The underprediction of but-1-ene-3-yne is due to the overconsumption of acetylene in the predicted result, which inhibits the formation of but-1-ene-3-yne. Propadiene and propyne are overpredicted for the entire range of $[A_S/V_R]$ ratios. These overvaluations are explained by the lack of the consumption reactions of propadiene and propyne. To our knowledge, the formation of pyrocarbon is accompanied by the production of hydrogen and the consumption of other gaseous species. The variations of light species as a function of $[A_S/V_R]$ ratio follow approximately a linear law. The simulated lines confirm to these rules. Except for propene, the simulated results of light species are all of the same order of magnitude compared to the experimental results, and the variation tendency of light species can be roughly revealed by the present simulated lines.

Figure 9 shows the predictions for the concentration profiles of hydrogen and acetylene as a function of temperature, compared to the experimental data from Marquaire et al.[11] Acceptable agreements between experimental and computational results of the molar fraction of gaseous species are realized. The acetylene molar fraction profiles as a function of temperature are well reproduced, while the prediction of hydrogen molar fraction is underestimated. In fact, the production of pyrocarbon leads to the consumption of acetylene and ethylene; therefore, the simulated concentrations of ethylene and acetylene with preform are lower than the simulated results without preform. Due to the dehydrogenation reactions from hydrocarbons, the molar fraction of hydrogen will increase.

4.3. Compositions of Heavy Gas-Phase Species. According to the experimental results of heavy species after 4 h of deposition from Marquaire et al.,[24] the molar fractions of heavy species at the outlet of the reactor are well estimated, as shown in Figure 10. The predictions of benzene, *p*-xylene, ethylbenzene, and cyclopentadiene are satisfying, while there are still some disparities in some range of the $[A_S/V_R]$ ratio. 1-Methylnaphthalene is overpredicted for the entire range of $[A_S/V_R]$ ratios, while 2-methylnaphthalene is overpredicted in $[A_S/V_R]$ ratios less than 40 cm^{-1} and underpredicted in higher $[A_S/V_R]$ ratios. The deviations might be caused by the lack of some gas-phase reaction pathways of the PAH formation and the incorrectness of the kinetic data. Overall, the molar fractions of heavy species decrease when the $[A_S/V_R]$ ratio increases. The simulated results of heavy species are all of the same order of magnitude compared to the experimental results, and the

dx.doi.org/10.1021/ie5026024 | Ind. Eng. Chem. Res. 2014, 53, 17537−17546

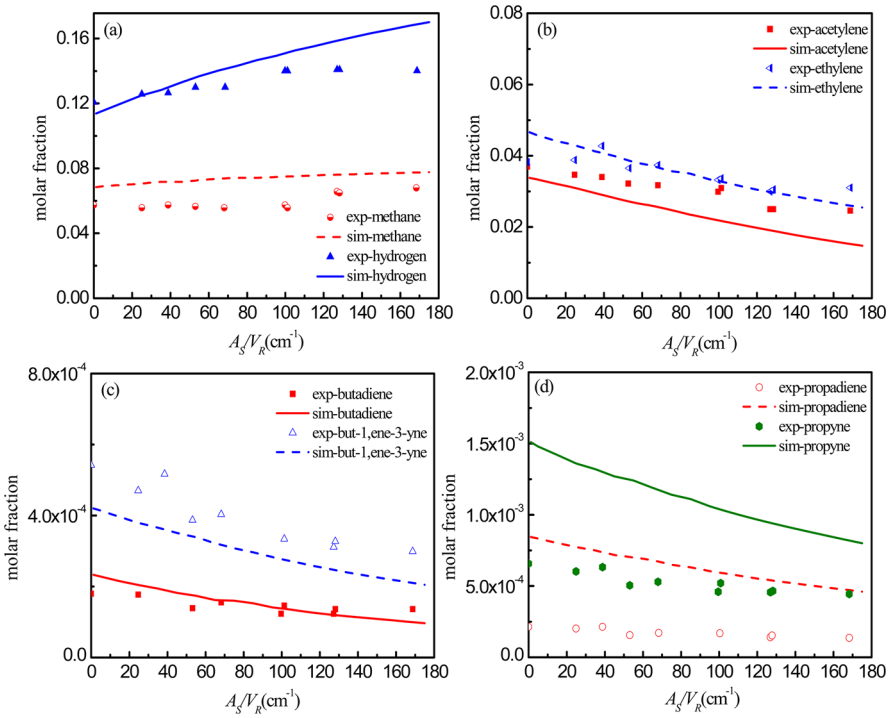

Figure 8. Influence of $[A_S/V_R]$ ratio on "light species" (symbols, experimental results; lines, simulated results).

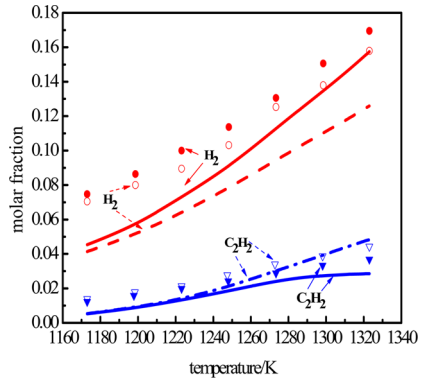

Figure 9. Hydrogen and acetylene mole fractions as a function of temperature (hollow symbols, experimental results without preform; solid symbols, experimental results with preform; solid lines, simulated results with preform; dashed line, dashed−dotted line, simulated results without preform).

variation tendency of heavy species can be roughly revealed by the present simulated lines.

Figure 11 shows the predictions for the concentration profiles of benzene and naphthalene as a function of temperature, compared to experimental data from Marquaire et al.[11] There are some numerical disparities between experimental and simulated results of the benzene and naphthalene molar fraction profiles as a function of temperature, while these values are of the same order of magnitude. There are two primary reasons for the deviations: first, an accurate heterogeneous reaction mechanism to express the pyrocarbon deposition process is still unavailable; second, the chemical kinetics database is still unavailable for all the elementary reactions (including gas-phase reactions and surface reactions).

4.4. Flow Rate Analysis. A flow rate analysis of propane pyrolysis in the CSTR module is presented at a temperature of 1273 K, a $[A_S/V_R]$ ratio of 45 cm^{-1}, and a residence time of 1 s, as shown in Figure 12. The arrows indicate the flow of consumption of a species, expressed as a percentage. The existence of surface reactions promotes the propane breaking up into methyl and ethyl. The methyl radicals are very active and are quickly consumed in the surface reactions, consequently accelerating the propane pyrolysis. Acetylene and ethylene are then largely adsorbed on the active carbon surface sites, which strongly inhibits the reactions in the gas phase. It is noticeable that a small amount of acetylene is consumed in the gas phase. The normalized rate-of-production coefficients higher than 5% are considered here, and the reaction pathways of propane pyrolysis are much simpler than the purely homogeneous reaction mechanism when surface reactions are included in the simulation. Figure 8 indicates that pyrocarbon is mostly produced by deposition of small unsaturated species (acetylene, ethylene), and methyl radicals play a key role in the pyrocarbon deposition.

5. CONCLUSIONS

The chemistry and kinetics of propane pyrolysis during the CVI process are modeled using elementary reactions consisting of 277 heterogeneous surface reactions with 72 surface species and 1074 homogeneous gas-phase reactions with 285 gas-phase species.[12] The heterogeneous reaction pathways and related surface reactions with corrected kinetic data are available in the Supporting Information. A prototype gas-phase reaction is chosen to match with the corresponding surface reaction, and the correction methods for three kinds of surface reactions (i.e., surface/gas reactions, unimolecular surface reactions, and surface/surface reactions) are proposed in this study. The time-dependent *continuous stirred tank reactor* (CSTR) module is applied to simulate propane pyrolysis in the perfectly stirred reactor. The propane pyrolysis with variations of the $[A_S/V_R]$ ratio from 5 to 175 cm^{-1} and a $[A_S/V_R]$ ratio of 1.1 cm^{-1} (without preform) are simulated here at 1273 K and a

dx.doi.org/10.1021/ie5026024 | *Ind. Eng. Chem. Res.* 2014, 53, 17537−17546

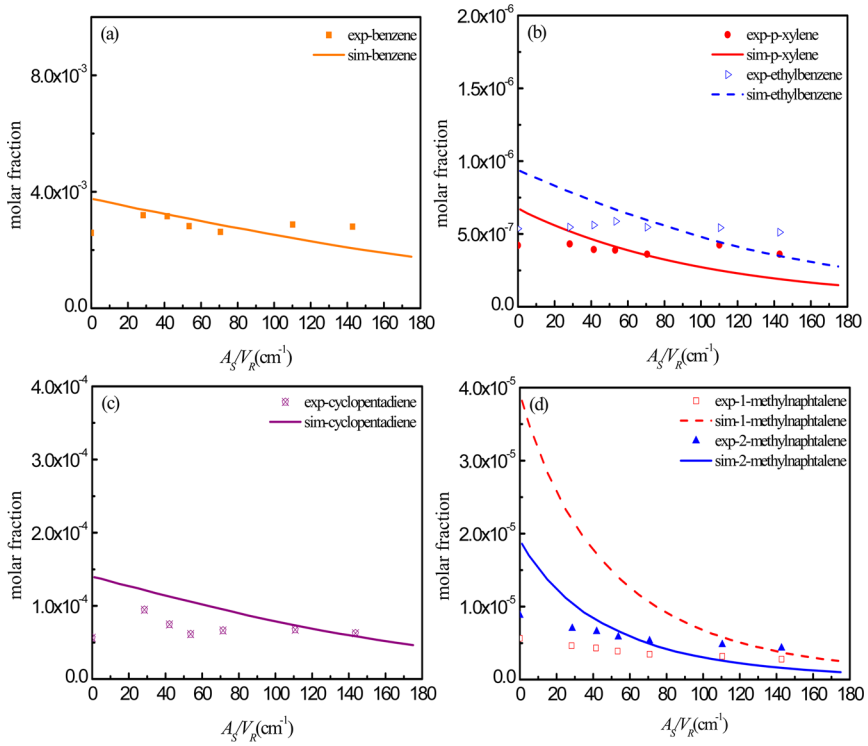

Figure 10. Influence of $[A_S/V_R]$ ratio on "heavy species" (symbols, experimental results, lines, simulated results).

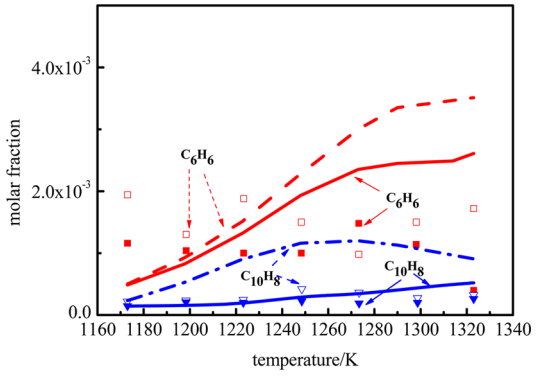

Figure 11. Benzene and naphthalene mole fractions as a function of temperature (hollow symbols, experimental results without preform; solid symbols, experimental results with preform; solid lines, simulated results with preform; dashed line, dashed−dotted line, simulated results without preform).

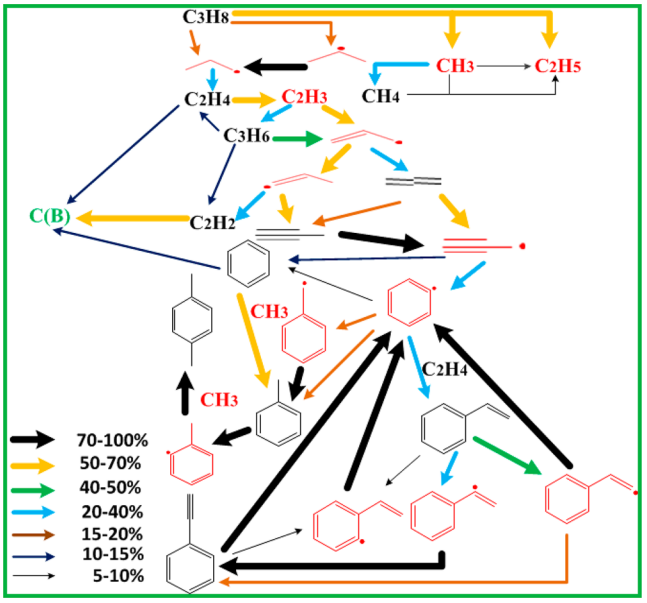

Figure 12. Flux analysis of propane pyrolysis (T = 1273 K, $[A_S/V_R]$ = 45 cm^{-1}, residence time = 1 s).

residence time of 1 s. In addition, gas-phase compositions and deposition kinetics of pyrocarbon are also predicted here at low pressure (2.6 kPa) with temperature ranging from 1173 to 1323 K, using propane diluted in nitrogen as precursor. Accepted agreements between the computational and experimental results of the concentration profiles of light hydrocarbon species and heavy hydrocarbon species, and the mass of pyrocarbon deposited as functions of the $[A_S/V_R]$ ratio and temperature are observed in the given conditions. The surface kinetic mechanism has merit in its generality without any adjustment of kinetic data of the surface elementary reactions. The compositions of gas-phase species and surface species vary as the $[A_S/V_R]$ ratio or temperature varies; consequently, there is a competitive relationship between the homogeneous gas-phase reactions and the heterogeneous surface reactions. According to the flow rate analysis, the main reaction pathways and gas-phase species during the propane pyrolysis emerged, as shown in Figure 12.

However, there is still a certain difference between the simulated and experimental results. The reasons are as follows: First, we are not able to propose a heterogeneous reaction mechanism consisting of the real reactions happening on the surface of carbon fibers; e.g., the formation of five-atom rings leading to the defects in the pyrocarbon needs to be considered in our further study. Second, accurate kinetic data of surface elementary reactions are not available at the current scientific level, and we still could not find reasonable theories as a strong

dx.doi.org/10.1021/ie5026024 | Ind. Eng. Chem. Res. 2014, 53, 17537−17546

support for the correction of kinetic data of the surface elementary reactions.

■ ASSOCIATED CONTENT

Supporting Information

Related information on the heterogeneous reaction mechanism for propane pyrolysis in the CVI process. This material is available free of charge via the Internet at http://pubs.acs.org.

■ AUTHOR INFORMATION

Corresponding Author

*E-mail: Aijun.Li@shu.edu.cn. Tel.: +8602156337502.

Notes

The authors declare no competing financial interest.

■ ACKNOWLEDGMENTS

Financial support from the Shanghai Science and Technology Commission for Grant 13521101202 and Grant 12520500300 is gratefully acknowledged. A.J.L. wishes to thank the Program for Professor of Special Appointment (Eastern Scholar) at Shanghai Institution of Higher Learning. The authors would also like to thank Prof. Deutschmann for the software support.

■ REFERENCES

(1) Sundaram, K. M.; Froment, G. F. Modeling of thermal cracking kinetics—I: Thermal cracking of ethane, propane and their mixtures. *Chem. Eng. Sci.* **1977**, *32*, 601−608.

(2) Delhaes, P. Chemical vapor deposition and infiltration processes of carbon materials. *Carbon* **2002**, *40*, 641−657.

(3) Kotlenski, W. V. In *Chemistry and Physics of Carbon*; Walker, P. L., Jr., Thrower, P. A., Eds.; Marcel Dekker, Inc.: New York, 1973; Vol. *9*, pp 173−262.

(4) Zhang, W.; Hüttinger, K. J. Chemical vapor infiltration of carbon—revised: Part I: Model simulations. *Carbon* **2001**, *39*, 1013−1022.

(5) Norinaga, K.; Deutschmann, O. Detailed Kinetic Modeling of Gas-Phase Reactions in the Chemical Vapor Deposition of Carbon from Light Hydrocarbons. *Ind. Eng. Chem. Res.* **2007**, *46*, 3547−3557.

(6) Norinaga, K.; Janardhanan, V. M.; Deutschmann, O. Detailed chemical kinetic modeling of pyrolysis of ethylene, acetylene, and propylene at 1073−1373 K with a plug-flow reactor model. *Int. J. Chem. Kinet.* **2008**, *40*, 199−208.

(7) Naslain, R.; Langlais, F. Fundamental and practical aspects of the chemical vapor infiltration of porous substrates. *High. Temp. Sci.* **1988**, *27*, 221−235.

(8) Descamps, C.; Vignoles, G. L.; Feron, O.; Langlais, F.; Lavenac, J. M. Correlation between homogeneous propane pyrolysis and pyrocarbon deposition. *J. Electrochem. Soc.* **2001**, *148*, 695−708.

(9) Ziegler, I.; Fournet, R.; Marquaire, P. M. Pyrolysis of propane for CVI of pyrocarbon: Part I. Experimental and modeling study of the formation of toluene and aliphatic species. *J. Anal. Appl. Pyrolysis* **2005**, *73*, 212−230.

(10) Ziegler, I.; Fournet, R.; Marquaire, P. M. Pyrolysis of propane for CVI of pyrocarbon: Part II. Experimental and modeling study of polyaromatic species. *J. Anal. Appl. Pyrolysis* **2005**, *73*, 231−247.

(11) Lacroix, R.; Fournet, R.; Ziegler, I.; Marquaire, P. M. Kinetic modeling of surface reactions involved in CVI of pyrocarbon obtained by propane pyrolysis. *Carbon* **2010**, *48*, 132−144.

(12) Xu, W.; Zhang, Z. W.; Bai, R. C.; Li, A. J.; Wang, J. S.; Sun, J. L. Kinetic Modeling of Gas-Phase Reactions for CVD from Propane. *New Carbon Mater.* **2014**, *29*, 67−77.

(13) Li, A.; Norinaga, K.; Zhang, W.; Deutschmann, O. Modeling and simulation of materials synthesis: Chemical vapor deposition and infiltration of pyrolytic carbon. *Compos. Sci. Technol.* **2008**, *68*, 1097−1104.

(14) Li, H.; Li, A.; Bai, R.; Li, K. Numerical simulation of chemical vapor infiltration of propylene into C/C composites with reduced multi-step kinetic models. *Carbon* **2005**, *43*, 2937−2950.

(15) Ziegler, I.; Fournet, R.; Marquaire, P. M. Pyrolysis of propane for CVI of pyrocarbon. *J. Anal. Appl. Pyrolysis* **2007**, *79*, 268−277.

(16) Becker, A.; Hüttinger, K. J. Chemistry and kinetics of chemical vapor deposition of pyrocarbon—II pyrocarbon deposition from ethylene, acetylene and 1,3-butadiene in the low temperature regime. *Carbon* **1998**, *36*, 177−199.

(17) Becker, A.; Hüttinger, K. J. Chemistry and kinetics of chemical vapor deposition of pyrocarbon—III pyrocarbon deposition from propylene and benzene in the low temperature regime. *Carbon* **1998**, *36*, 201−211.

(18) Becker, A.; Hüttinger, K. J. Chemistry and kinetics of chemical vapor deposition of pyrocarbon—IV pyrocarbon deposition from methane in the low temperature regime. *Carbon* **1998**, *36*, 213−224.

(19) Frenklach, M.; Wang, H. Detailed surface and gas-phase chemical kinetics of diamond deposition. *Phys. Rev. B* **1991**, *43*, 1520−1545.

(20) Wauters, S.; Marin, G. B. Kinetic Modeling of Coke Formation during Stream Cracking. *Ind. Eng. Chem. Res.* **2002**, *41*, 2379−2391.

(21) Zhang, W.; Hüttinger, K. J. Chemical vapor deposition of carbon from methane at various pressures, partial pressures and substrate surface area/reactor volume ratios. *J. Mater. Sci.* **2001**, *36*, 3503−3510.

(22) Hu, Z.; Zhang, W.; Hüttinger, K. J.; Reznik, B.; Gerthsen, D. Influence of pressure, temperature and surface area/volume ratio on the texture of pyrolytic carbon deposited from methane. *Carbon* **2003**, *41*, 749−758.

(23) Hu, Z.; Hüttinger, K. J. Influence of the surface area/volume ratio on the chemistry of carbon deposition from methane. *Carbon* **2003**, *41*, 1501−1508.

(24) Ziegler, I.; Fournet, R.; Marquaire, P. M. Influence of surface on chemical kinetic of pyrocarbon deposition obtained by propane pyrolysis. *J. Anal. Appl. Pyrolysis* **2005**, *73*, 107−115.

(25) Deutschmann, O.; Tischer, S.; Correa, C.; Chatterjee, D.; Kleditzsch, S.; Janardhanan, V. *DETCHEM Software Package*; version 2.1; 2007.

(26) Cuesta, A.; Dhamelincourt, P.; Laureyns, J.; Martinez, A. A.; Tascon, J. M. D. Raman microprobe studies on carbon materials. *Carbon* **1994**, *32*, 1523−1532.

(27) Compagnini, G.; Puglisi, O.; Foti, G. Raman spectra of virgin and damaged graphite edge planes. *Carbon* **1997**, *35*, 1793−1797.

(28) Biro, L. P.; Lambin, P. Grain boundaries in graphene grown by chemical vapor deposition. *New J. Phys.* **2013**, *15*, 035024.

(29) Cervenka, J.; Flipse, C. Structural and electronic properties of grain boundaries in graphite: Planes of periodically distributed point defects. *Phys. Rev. B* **2009**, *79*, No. 195429.

(30) Huang, P. Y.; Ruiz-Vargas, C. S.; van der Zande, A. M.; Whitney, W. S.; Levendorf, M. P.; Kevek, J. W.; Garg, S.; Alden, J. S.; Hustedt, C. J.; Zhu, Y.; Park, J.; McEuen, P. L.; Muller, D. A. Grains and Grain Boundaries in Single-Layer Graphene Atomic Patchwork Quilts. *Nature* **2011**, *469*, 389−392.

(31) Froment, G. F.; Bischoff, K. B. *Chemical Reactor Analysis and Design*; John Wiley and Sons: New York, 1979.

(32) Baxter, R. J.; Hu, P. Insight into why the Langmuir−Hinshelwood mechanism is generally preferred. *J. Chem. Phys.* **2002**, *116*, 4379−4381.

(33) Bohm, H.; Jander, H.; Tanke, D. PAH Growth and Soot Formation in the Pyrolysis of Acetylene and Benzene at High Temperatures and Pressures. *Proc. Combust. Inst.* **1998**, *27*, 1605−1612.

(34) Dong, G.; Hüttinger, K. J. Consideration of reaction mechanisms leading to pyrolytic carbon of different textures. *Carbon* **2002**, *40*, 2515−2528.

(35) Norinaga, K.; Deutschmann, O.; Saegusa, N.; Hayashi, J. I. Analysis of Pyrolysis Products from Light Hydrocarbons and Kinetic Modeling for Growth of Polycyclic Aromatic Hydrocarbons with Detailed Chemistry. *J. Anal. Appl. Pyrolysis* **2009**, *86*, 148−160.

(36) Violi, A.; Truong, T. N.; Sarofim, A. F. Kinetics of Hydrogen Abstraction Reactions from Polycyclic Aromatic Hydrocarbons by H Atoms. *J. Phys. Chem. A* **2004**, *108*, 4846−4852.
(37) Hu, Z.; Schoch, G.; Hüttinger, K. J. Chemistry and kinetics of chemical vapor infiltration of pyrocarbon: VII: infiltration of capillaries of equal size. *Carbon* **2000**, *38*, 1059−1065.
(38) Glasier, G. F.; Filfil, R.; Pacey, P. D. Formation of polycyclic aromatic hydrocarbons coincident with pyrolytic carbon deposition. *Carbon* **2001**, *39*, 497−506.
(39) Tokmakov, I. V.; Lin, M. Reaction of phenyl radicals with acetylene: Quantum chemical investigation of the mechanism and master equation analysis of the kinetics. *J. Am. Chem. Soc.* **2003**, *125*, 11397−11408.
(40) Richter, H.; Howard, J. B. Formation and consumption of single-ring aromatic hydrocarbons and their precursors in premixed acetylene, ethylene and benzene flames. *Phys. Chem. Chem. Phys.* **2002**, *4*, 2038−2055.
(41) Baulch, D. L.; Cobos, C. J.; Cox, R. A. Evaluated kinetic data for combustion modelling. *J. Phys. Chem. Ref. Data* **1992**, *21*, 411−429.
(42) Dean, A. Predictions of Pressure and Temperature Effects Upon Radical-Addition and Recombination Reactions. *J. Phys. Chem.* **1985**, *89*, 4600−4608.
(43) Harding, L. B.; Georgievskii, Y.; Klippenstein, S. J. Predictive theory for hydrogen atom−hydrocarbon radical association kinetics. *J. Phys. Chem. A* **2005**, *109*, 4646−4656.
(44) Wang, H.; Frenklach, M. Calculations of Rate Coefficients for the Chemically Activated Reactions of Acetylene with Vinylic and Aromatic Radicals. *J. Phys. Chem.* **1994**, *98*, 11465−11489.
(45) Zhang, W. G.; Hu, Z. J.; Huttinger, K. J. Chemical vapor infiltration of carbon fiber felt: optimization of densification and carbon microstructure. *Carbon* **2002**, *40*, 2529−2545.